The Journal of Chemical Physics

Permutation invariant polynomial neural network approach to fitting potential energy surfaces. IV. Coupled diabatic potential energy matrices

Cite as: J. Chem. Phys. **149**, 144107 (2018); https://doi.org/10.1063/1.5054310
Submitted: 30 August 2018 . Accepted: 19 September 2018 . Published Online: 09 October 2018

Changjian Xie, Xiaolei Zhu, David R. Yarkony, and Hua Guo

Permutation invariant polynomial neural network approach to fitting potential energy surfaces. IV. Coupled diabatic potential energy matrices

Changjian Xie,[1] Xiaolei Zhu,[2,a)] David R. Yarkony,[2] and Hua Guo[1,b)]
[1]*Department of Chemistry and Chemical Biology, University of New Mexico, Albuquerque, New Mexico 87131, USA*
[2]*Department of Chemistry, Johns Hopkins University, Baltimore, Maryland 21218, USA*

(Received 30 August 2018; accepted 19 September 2018; published online 9 October 2018)

A machine learning method is proposed for representing the elements of diabatic potential energy matrices (PEMs) with high fidelity. This is an extension of the so-called permutation invariant polynomial-neural network (PIP-NN) method for representing adiabatic potential energy surfaces. While for one-dimensional irreducible representations the diagonal elements of a diabatic PEM are invariant under exchange of identical nuclei in a molecular system, the off-diagonal elements require special symmetry consideration, particularly in the presence of a conical intersection. A multiplicative factor is introduced to take into consideration the particular symmetry properties while maintaining the PIP-NN framework. We demonstrate here that the extended PIP-NN approach is accurate in representing diabatic PEMs, as evidenced by small fitting errors and by the reproduction of absorption spectra and product branching ratios in both $H_2O(\tilde{X}/\tilde{B})$ and $NH_3(\tilde{X}/\tilde{A})$ non-adiabatic photodissociation. *Published by AIP Publishing.* https://doi.org/10.1063/1.5054310

I. INTRODUCTION

The Born-Oppenheimer (BO) approximation,[1] which separates the fast motion of electrons from that of the slow nuclei, forms a cornerstone of modern theoretical chemistry. In this adiabatic representation, the electronic energy is obtained by the *ab initio* solution of the electronic Schrödinger equation at a fixed nuclear geometry. Indeed, this is now done on a routine basis in quantum chemical calculations. The resulting *ab initio* points can be envisaged to form an analytical function of nuclear coordinates, referred to as an adiabatic potential energy surface (PES). The solution of the nuclear Schrödinger equation on the PES yields dynamical attributes such as molecular spectra and/or reaction cross sections/rate constants, which can be compared directly with experimental measurements. As such, the PES serves as a key bridge between the electronic structure and nuclear dynamics.

For a molecular system with N atoms, the PES has $3N$-6 dimensions. In the early days of PES development, mostly empirical data were used.[2] Now, the advances in *ab initio* theory have made it possible to compute many points throughout the relevant configuration space. However, representing the discrete data set, consisting of electronic structure attributes (energies, energy gradients, and derivative couplings), computed at many nuclear configurations with an analytic multi-dimensional function is not a trivial undertaking. In addition to the requisite high fidelity of the fitting over a large number of molecular configurations, it is also important to enforce the permutation symmetry of the PES for exchanging identical nuclei in the molecule. Recently, there have been remarkable advances in developing global adiabatic PESs for reactive systems from *ab initio* data.[3–9] Particularly noteworthy is the use of machine learning methods, such as neural networks (NNs), in constructing high-dimensional PESs.[10–14] Permutation symmetry can be effectively enforced either through an atomistic NN framework[15,16] or by front-loading the NN with polynomial symmetry functions.[17–19] The latter is called the permutation invariant polynomial-neural network (PIP-NN) approach.[12,17,18,20] The high accuracy of *ab initio* calculations and high fidelity fitting of the PESs have greatly advanced our understanding of molecular spectroscopy and reaction dynamics,[21,22] as evidenced by some of the most recent elucidations of state-of-the-art experiments.[23–26]

Despite its effectiveness, it is long realized that the BO approximation fails near an electronic degeneracy, such as a conical intersection (CI).[27,28] Non-adiabatic coupling terms (NACTs), such as the derivative coupling, allow transitions among different electronic states, which breaks the BO single PES construct. While non-adiabatic dynamics can be formally treated within a multi-state adiabatic representation, numerically it is difficult because of the singularities of the NACTs at the electronic degeneracy.[29] An analytic representation of an adiabatic PES near a discontinuity, such as a cusp, is also challenging. Furthermore, the adiabatic representation requires the inclusion of the geometric phase,[30] which is known to play an important role in dynamics.[31–33] In particular, it is recently shown that even at energies much lower than that of the CI the geometric phase can strongly influence the adiabatic dynamics.[34–36] For dynamical calculations, it is thus preferable to use a diabatic representation because the corresponding potentials are smooth with the singularities removed.[37–40]

a)Present address: Department of Chemistry, Stanford University, Stanford, CA 94305, USA.
b)Author to whom correspondence should be addressed: hguo@unm.edu

The diabatic representation is formally a unitary transformation of the adiabatic representation, in which the derivative coupling is eliminated.[29] This adiabatic-to-diabatic (AtD) transformation converts adiabatic PESs to a diabatic potential energy matrix (PEM), in which the diagonal terms represent the diabatic PESs, while the off-diagonal terms are the electronic couplings, replacing the derivative couplings in the adiabatic representation. Both the diagonal and off-diagonal elements of the PEM are smooth functions of nuclear coordinates and can thus be readily expressed by analytic functions. There are many different strategies for diabatization.[39,41] Some are based on explicit minimization of the derivative coupling,[42–45] having the advantage that the quality of the diabatization can be quantified, while others are based on molecular properties[46–49] or simply by an ansatz.[37,50,51] It should be noted however that complete removal of the NACTs is not possible for polyatomic systems,[52,53] so diabatization always contains some uncertainties and is thus not unique.

There has been much less discussion on constructing diabatic PEMs from *ab initio* adiabatic state data than that for adiabatic PES, mainly because of complications associated with diabatization. Recently, however, there has been increased activity in this area for both bound and reactive systems.[43,44,50,54–63] In particular, Collins and co-workers developed a scheme based on modified Shepard interpolation, in which the local diabatic PEM elements are determined self-consistently from adiabatic energies, gradients, and derivative couplings.[43,54,55] Two of the current authors also advanced a global scheme to directly fit the same adiabatic data with the diabatic PEM expressed in symmetry adapted polynomials.[44,58,59] Very recently, attempts have been made to represent PEMs with NNs in order to achieve higher fitting accuracy,[64,65] but issues remain, particularly with respect to the adaptation of permutation symmetry.

In this work, we focus on a high-fidelity representation of the diabatic PEM using NNs by extending the PIP-NN approach. Our assumption here is that diabatization has already been carried out, and the goal is to analytically represent both the diagonal and off-diagonal elements of the diabatic PEM already determined at various nuclear geometries. This approach is thus different from the recent work of Lenzen and Manthe,[64] who fit the adiabatic energies alone with a NN-based PEM within an ansatz based diabatization framework in which the derivative coupling is not used in the fitting. Although both the energy and derivative coupling were used to fit a diabatic NN-based PEM, the work of Guan *et al.* was restricted to an avoided crossing between two electronic states, in which case no symmetry issues arise.[65] In this work, we discuss the specific issues in NN fitting of PEMs associated with CIs and devise appropriate functional forms within the PIP-NN framework. Two examples are employed to illustrate the method, in which the corresponding CIs figure prominently in their photodissociation dynamics. In addition to fitting errors, photoabsorption spectra and product branching ratios are used to validate the new PIP-NN PEMs. These tests demonstrated the accuracy of the new approach. This work is organized as follows. The general strategy and implementation are discussed in Sec. II. The test results for H_2O and NH_3 are presented in Sec. III. Finally, conclusions and prospects are given in Sec. IV.

II. PEM FITTING

A. Adiabatic and diabatic representations

We focus here on a two-state model, in which the diabatic PEM is a 2×2 matrix

$$V^{(d)} = \begin{pmatrix} V_{11} & V_{12} \\ V_{12} & V_{22} \end{pmatrix}. \tag{1}$$

Here, V_{11}, V_{22}, and V_{12} are the diabatic PESs and coupling potential, respectively. In such a two-state system, V_{11}, V_{22}, and V_{12} can be obtained from the adiabatic potentials (W_- and W_+) by the following unitary transformation:

$$U = \begin{pmatrix} \cos\alpha & -\sin\alpha \\ \sin\alpha & \cos\alpha \end{pmatrix} \tag{2}$$

and can be written as

$$V_{11} = W_-\cos^2\alpha + W_+\sin^2\alpha, \tag{3a}$$

$$V_{22} = W_-\sin^2\alpha + W_+\cos^2\alpha, \tag{3b}$$

$$V_{12} = \frac{1}{2}(W_+ - W_-)\sin 2\alpha, \tag{3c}$$

where α is the AtD transformation (or mixing) angle

$$\alpha = \frac{1}{2}\arctan\frac{2V_{12}}{V_{11} - V_{22}}, \tag{4}$$

which is dependent on the nuclear coordinates. The adiabatic potentials W_- and W_+ can be computed at relevant nuclear geometries using an *ab initio* method directly, and the corresponding AtD angle is assumed to have been obtained through some form of diabatization. For systems with more than two states, we can also assume that the AtD transformation matrix exists and the elements of the diabatic PEM are obtainable from adiabatic calculations, albeit in a discrete form. Since we are mostly concerned with the methodology in this work, we choose to demonstrate the technique by representing points generated from the known analytic diabatic PEMs for two polyatomic systems, namely, $H_2O(\tilde{X}/\tilde{B})$[66,67] and $NH_3(\tilde{X}/\tilde{A})$.[68,69]

The diagonal elements V_{11} and V_{22} are invariant under exchange of identical nuclei in the molecule and thus can be directly and separately fitted using the PIP-NN method (*vide infra*). However, for the coupling potential V_{12}, the permutation symmetry relates to the symmetries of the two coupled electronic states. Its symmetry needs to be carefully considered in the fitting. The relevant symmetry is the complete nuclear permutation and inversion (CNPI) group,[70] as discussed extensively in the literature.[43,44,50,56] In addition, its behavior near a CI is further constrained by the geometric phase. These two points are discussed in Subsections II B and II C.

B. Symmetry consideration

We first discuss the non-adiabatically coupled $\tilde{X}^1A'$ and $\tilde{B}^1A'$ states of H_2O responsible for its photodissociation in the B band. These two states form two seams of CIs located at the

linear configurations ($C_{\infty v}$) HHO and HOH,[71–73] in which the ground and excited electronic states have $^1\Pi$ and $^1\Sigma^+$ point group symmetries, respectively. The CNPI group in question is the direct-product group of the symmetric group of order 2 S_2 (which permutes the two hydrogen nuclei) and the inversion group $i = (E, E^*)$ where E^* inverts all particles, both electrons and nuclei, through the origin. This CNPI group is isomorphic to the C_{2v} point group and we will refer to it by the name CNPI(C_{2v}), although we emphasize that their elements are different. For C_{2v} point group geometries, the group operations are equivalent (see Table I and Ref. 70) and we can determine the irreducible representations carried by the two electronic states. To this end, we choose the H_2O equilibrium geometry on the ground electronic state. This choice is arbitrary as it is assumed that the slowly changing diabatic states should have the same symmetry in all configuration space. At this C_{2v} geometry, both the $\tilde{X}$ (V_{11}) and $\tilde{B}$ (V_{22}) states of H_2O belong to the A_1 irreducible representation of the CNPI(C_{2v}) group. As a result, the coupling term (V_{12}) belongs to the $A_1 \times A_1 = A_1$ irreducible representation, as it represents the off-diagonal potential matrix element between two A_1 states. As shown in Table I, the totally symmetric A_1 irreducible representation has a +1 character under permutation operation (12), so the V_{12} term should be symmetric with respect to the exchange of the two H atoms.

For the NH_3 case, the *A* band photodissociation involves the ground and first excited states ($\tilde{X}^1A_1'$ and $\tilde{A}^1A_2''$). The minimal energy CI formed between these two electronic states is planar and has C_{2v} point group symmetry.[44,56,74] The CNPI group of NH_3 is the direct product of the symmetric group of order 3 for the 3 hydrogen nuclei S_3, and the inversion group (i), given above, and is isomorphic to the D_{3h} point group; we will refer to this group as CNPI(D_{3h}). Note that as seen in Table II there is an equivalence between the point group and CNPI group operations at D_{3h} point group geometries, which enables the identification of the CNPI irreducible representation labels of the electronic states. To determine the CNPI symmetry of V_{12}, we examine the electronic states at the equilibrium geometry of the excited state, again conveniently chosen. At this D_{3h} point group symmetry geometry, the $\tilde{X}$ (V_{11}) and $\tilde{A}$ (V_{22}) electronic states belong to the A_1' and A_2'' irreducible representations of the CNPI group, respectively. Thus, V_{12} belongs to the $A_1' \times A_2'' = A_2''$ irreducible representation. As shown in Table II, V_{12} is symmetric with respect to the (123 → 231) and (123 → 312) permutations, while antisymmetric with respect to the (123 → 213), (123 → 321), and (123 → 132) permutations. In other words, it is antisymmetric with exchange of two H atoms.

TABLE I. Character table of the CNPI group for H_2O and point group C_{2v}. E: identity; (12): the permutation of two identical nuclei numbered 1 and 2; E^*: inversion; $(12)^*$: inversion after doing (12).[70]

CNPI	E	(12)	$(12)^*$	E^*
C_{2v}	E	C_2	σ_h	σ_v
A_1	1	1	1	1
A_2	1	1	−1	−1
B_1	1	−1	1	−1
B_2	1	−1	−1	1

TABLE II. Character table of the CNPI group for NH_3 and point group D_{3h}. Operation (abc): the permutation replacing a by b, b by c, and c by a.[70]

CNPI	E	(123) (132)	(12) (23) (13)	E^*	$(123)^*$ $(132)^*$	$(12)^*$ $(23)^*$ $(13)^*$
D_{3h}	E	$2C_3$	$3C_2$	σ_h	$2S_3$	$3\sigma_v$
A_1'	1	1	1	1	1	1
A_2'	1	1	−1	1	1	−1
E'	2	−1	0	2	−1	0
A_1''	1	1	1	−1	−1	−1
A_2''	1	1	−1	−1	−1	1
E''	2	−1	0	−2	1	0

C. Conical intersections

Apart from the permutation symmetry discussed above, the coupling term V_{12} has to satisfy an additional constraint near the CI. In particular, the line integral of the derivative coupling τ along a closed loop around a CI should yield a value π[75]

$$\oint_\Gamma \boldsymbol{\tau}(\mathbf{s}|\Gamma) \cdot d\mathbf{s} = \pi, \tag{5}$$

where Γ denotes the closed integral path and $\boldsymbol{s}$ is a point on the path. This corresponds to the geometric phase. For a complete circle, $e^{i\pi} = -1$, which means that a real adiabatic electronic wavefunction changes sign when encircling the CI.[30] To assure continuity of the parameters along the seam of intersection, the coordinates s are taken as the polar coordinates of the (x, y) axis formed by the orthogonal $\boldsymbol{g}$ and $\boldsymbol{h}$ vectors that define the branching space of the CI. Here, $\boldsymbol{g}$ (the tuning mode) is the energy difference gradient vector and $\boldsymbol{h}$ (the coupling mode) is the coupling gradient vector,[27,76] which lift the degeneracy at first order in displacements. It should be noted that the loops surrounding more than one CI are not considered in this work.

Equation (5) holds regardless of the path, as long as it encircles the CI and the derivative coupling is removable[77] (which is the case here), or the path is infinitesimal. Thus, one can simplify the path Γ with a small circle centered at the CI with a small radius ρ along the polar angle φ and then Eq. (5) becomes[73]

$$\int_0^{2\pi} \tau(\varphi|\rho) d\varphi = \pi. \tag{6}$$

In the following, we will discuss the implications of Eq. (6) in both molecules near their respective CIs.

Along the closed circle, the diagonal elements of the diabatic PEM, V_{11} and V_{22}, are both symmetric with respect to $\varphi = \pi$ for φ varying from 0 to 2π. Thus, their derivatives $\partial V_{11}/\partial\varphi$ and $\partial V_{22}/\partial\varphi$ are antisymmetric for $\varphi \in [0, 2\pi]$. For the coupling term V_{12}, on the other hand, its symmetry with respect to $\varphi = \pi$ is dictated by that of the projection of derivative coupling along the direction of $d\varphi$, which is symmetric with respect to $\varphi = \pi$, since an antisymmetric τ leads the integral

in Eq. (6) to zero. From Eq. (4), one can express the derivative coupling as follows:[78]

$$\tau(\varphi|\rho) = \frac{\partial\alpha}{\partial\varphi} = \frac{1}{2}\cdot\frac{1}{1+\left(\frac{2V_{12}}{V_{11}-V_{22}}\right)^2} \cdot\frac{2\left[\frac{\partial V_{12}}{\partial\varphi}(V_{11}-V_{22}) - V_{12}\left(\frac{\partial V_{11}}{\partial\varphi}-\frac{\partial V_{22}}{\partial\varphi}\right)\right]}{(V_{11}-V_{22})^2}. \quad (7)$$

It follows that the coupling term V_{12} has to be antisymmetric with respect to $\varphi = \pi$ and $\partial V_{12}/\partial\varphi$ needs be symmetric because $\partial V_{11}/\partial\varphi$ and $\partial V_{22}/\partial\varphi$ are antisymmetric (as shown below in two systems H_2O and NH_3).

For the H_2O case, the HOH or HHO bending mode is the coupling mode and the H–O or H–H stretching mode is the tuning mode. We will only consider the HOH CI here, as the treatment of the HHO one is the same. A small circle within the HOH′ molecular plane enclosing the HOH′ CI is shown in Fig. 1(a), which includes both the tuning and coupling modes (in the ***g***-***h*** branching space). This circle can be defined by a small fixed radius ρ and the angle $\varphi \in (0, 2\pi)$. Note that both $\varphi = 0$ and π correspond to the HOH′ linearity, so the HOH′ angle θ needs be defined in the range $(0, 2\pi)$ within the plane. This is not necessary for the dynamical calculations where $\theta \in (0, \pi)$, but important for the behavior of V_{12} near linearity. Near linearity, as discussed above, the derivative coupling is symmetric with respect to φ, which means that V_{12} has to be antisymmetric with respect to φ. It follows that the symmetry of V_{12} is antisymmetric with respect to θ as well. To guarantee the proper behavior of the coupling term V_{12} near linearity, we introduce a multiplicative factor $(\sin\theta)$ that is antisymmetric with respect to θ near linearity. The remainder of the coupling is thus symmetric with respect to θ. In practice, we chose to fit

$$V'_{12} = \frac{V_{12}}{\sin\theta} \quad (8)$$

instead of V_{12}. In the end, V'_{12} needs to be multiplied by $\sin\theta$ to recover V_{12}. This treatment makes V_{12} exactly zero at the linear configuration ($\sin\theta = 0$) with the proper asymptotic linear dependence of the angle near linearity. This is not the case if the $\sin\theta$ term is not included, such as in the previous spline fit (*vide infra*).[67] It should be noted that in this fitting method, the angle θ is sampled within the range of $(0, \pi)$, in which V'_{12} is invariant with respect to the permutation of two identical nuclei because V_{12} is invariant as discussed above and amenable to the PIP-NN method. Furthermore, no points were chosen at linear configurations to avoid the singularities in Eq. (8).

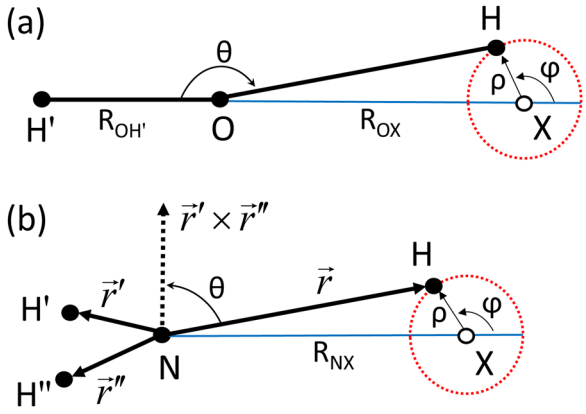

FIG. 1. Illustration of the closed loop used to perform the line integral around the collinear HOH CI in H_2O (a) and the C_{2v} CI in NH_3 (b). The former is within the molecular plane, while the latter is in a plane perpendicular to the H′NH″ plane.

For the more complex system NH_3, the circular path for the line integral in Eq. (6) can be defined in the plane that contains the dissociating N–H and bisects the H′NH″ angle, as shown in Fig. 1(b). This path encircles the CI in the branching space spanning by the coupling (umbrella angle, θ) and tuning (N–H bond) modes. The corresponding angle (φ) defines the planarity at 0 and π, which corresponds to $\theta = \pi/2$. The umbrella angle (θ) of NH_3 is naturally defined between 0 and π. Using the same arguments presented above for H_2O, the coupling term V_{12} has to be antisymmetric near planarity with respect to φ as well as θ. For this system, hence, the following function is used in the PIP-NN fitting:

$$V'_{12} = \frac{V_{12}}{\gamma}, \quad (9)$$

where γ relates to the geometry deviating from the planar point[44,79]

$$\gamma = \left(\frac{\mathbf{r}'\times\mathbf{r}''\cdot\mathbf{r}}{|\mathbf{r}'||\mathbf{r}''||\mathbf{r}|}\right), \quad (10)$$

in which $\mathbf{r}$, $\mathbf{r}'$, and $\mathbf{r}''$ are the bond distance vectors as shown in Fig. 1(b). Again, V_{12} is recovered by multiplying V'_{12} by γ after the fitting. It is clear from Eq. (10) that $\gamma = 0$ corresponds to the planar geometries of NH_3. When any two identical H atoms are exchanged, γ changes its sign. As discussed above, V_{12} is antisymmetric with the permutation of the two H atoms. As a result, V'_{12} becomes invariant with respect to the exchange of the two H atoms and thus amenable to the PIP-NN method.

D. Fitting of PEMs within the PIP-NN framework

Since the details of the PIP-NN method can be found in earlier publications,[12,17,18] we present here only a brief description. The invariance of an adiabatic PES under permutation of identical nuclei is enforced in the PIP-NN method by using low-order permutation invariant polynomials (PIPs)[5] as the input layer of the NN. The symmetrized polynomials are defined as follows:[80]

$$G = \hat{S}\prod_{i<j}^{N} p_{ij}^{l_{ij}}, \quad (11)$$

where l_{ij} is the order of the monomial, $\hat{S}$ is the symmetrization operator, N is the number of nuclei, and $p_{ij} = \exp(-\alpha r_{ij})$ are the Morse-like variables with the parameter $\alpha = 2/3$ Å^{-1} and the internuclear distances r_{ij}.

The NN fittings were trained using the Levenberg-Marquardt algorithm[81] using the root mean square error (RMSE) as the penalty function

$$\mathrm{RMSE} = \sqrt{\sum_{i=1}^{N_{\mathrm{data}}}\left(E_i^{\mathrm{output}} - E_i^{\mathrm{target}}\right)^2/N_{\mathrm{data}}}, \quad (12)$$

where E_i^{target} and E_i^{output} are the input and fitted energies, respectively. To avoid overfitting, the data are randomly

divided into three sets, namely, the training (90% of the data points), validation (5%), and testing (5%) sets. Because of non-linear nature of the minimization, many optimization runs were performed and the final result is obtained with the smallest RMSE. 200 different training calculations were performed, and the "early stopping" method was used to avoid overfitting.[10]

III. RESULTS AND DISCUSSION

For the H_2O system, 6210 *ab initio* points chosen in Ref. 67 were used to fit the diabatic PEM elements V_{11}, V_{22}, and V_{12} in the three dimensions. Three PIPs up to the second order for this AB_2 system and 20 neurons in each of the two hidden layers were used in the NN fitting. The fitting RMSEs for the diagonal V_{11} and V_{22} terms are 4.7 and 8.2 meV, respectively. The RMSE for V_{12} is 6.4 meV. Figure 2 shows the fitting error distributions for V_{11}, V_{22}, and V_{12}. The errors are quite evenly distributed in large energy ranges (~15 and ~4 eV for the diagonal and off-diagonal terms, respectively).

To further examine the accuracy of the diabatic PES fitted by the extended PIP-NN method, we performed quantum dynamics calculations on the PIP-NN PEM and compared the results with those on the spline PEM.[67] The details of the calculations can be found in our earlier work,[67] and the parameters in the calculations are listed in Table III. Figure 3 (upper panel) shows the absorption spectrum for the ground ro-vibrational initial state of H_2O using the original spline[67] and the new PIP-NN PEMs. It can be readily seen that the absorption spectrum calculated on new diabatic PEM reproduces that on the

TABLE III. Numerical parameters (in a.u.) used in wave packet calculations for the H_2O photodissociation in the B band.

Grid/basis ranges and sizes
$r \in [1.0, 6.0]$, $N_r = 85$; $R \in [1.0, 16.0]$, $N_R = 155$
$N_j = 70$ over [0°, 180°];
Damping functions
$\exp[-0.03(r - 4.0)^2]$, for $4.0 < r < 6.0$
$\exp[-0.02(R - 12.3)^2]$, for $12.3 < R < 16.0$
Chebyshev propagation steps: 15 000

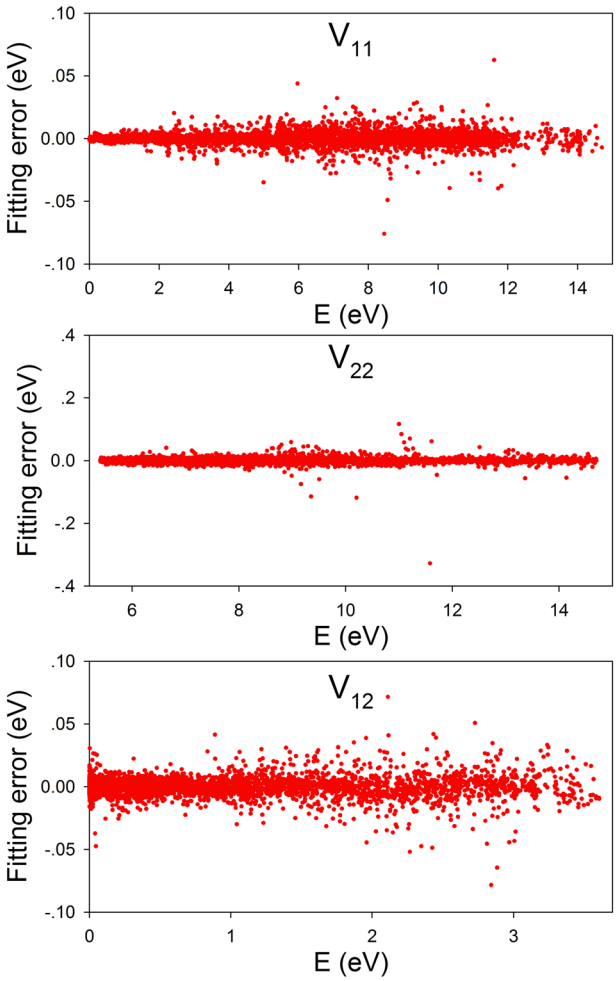

FIG. 2. Distributions of fitting errors for the V_{11}, V_{22}, and V_{12} of the H_2O PEM.

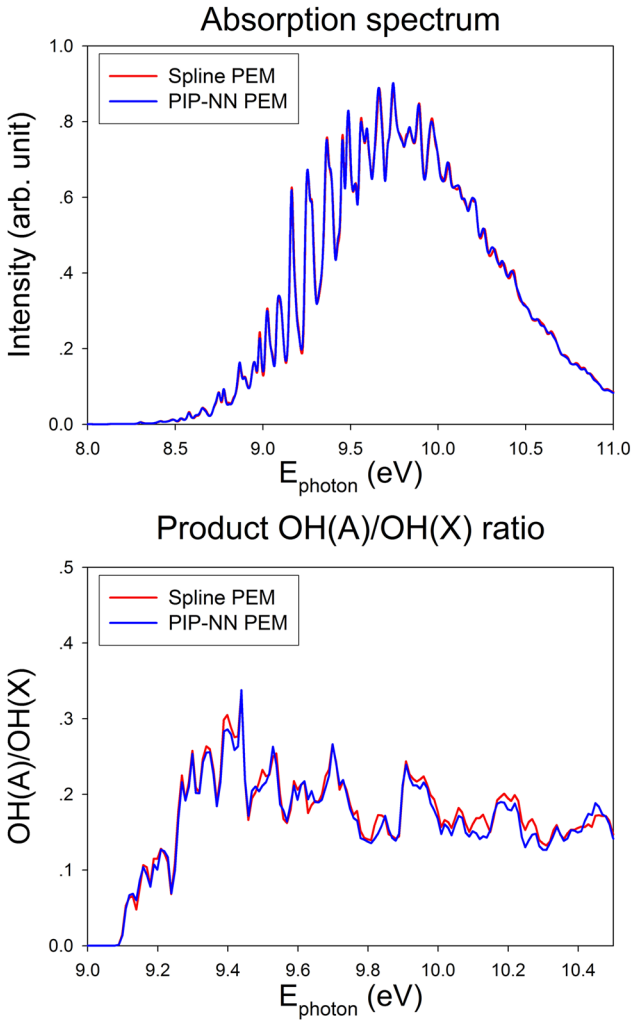

FIG. 3. Comparison of the calculated absorption spectrum (upper panel) and OH($\tilde{A}$)/OH($\tilde{X}$) branching ratio (lower panel) as a function of the photon energy (in eV) in the B band photodissociation of H_2O, using the spline[67] and PIP-NN PEMs.

spline PEM almost perfectly, down to every detail, suggesting high accuracy of the PIP-NN method. Furthermore, the product OH($\tilde{A}$)/OH($\tilde{X}$) branching ratio, which is largely controlled by non-adiabatic transitions near the HOH CI, was also computed over an energy range. As shown in Fig. 3 (lower panel), the branching ratio calculated on the PIP-NN PEM is also in good agreement with that on the spline PEM, including the oscillatory structures and widths of the peaks. The good agreement further validates the high accuracy of V_{12} fitted by the PIP-NN method.

As discussed above, the HOH bending angle θ is extended to [0, 2π] to satisfy the requirement that the line integral of the derivative coupling τ along a closed loop around a CI yields a value of π. Figure 4(a) shows V_{12} as a function of φ encircling the CI [the open dot in Fig. 1(a), $R_{OH'}$ = 1.8 bohr, R_{OX} = 3.165 bohr (X = H), and ρ = 0.6 bohr] on the PIP-NN and the previous spline PEMs. It can be seen that the PIP-NN V_{12} term changes sign when passing through linearity, while V_{12} in the previous spline PEM approaches zero at linearity because of its restriction of the angle θ from 0 to π. Figure 4(b) shows the corresponding non-adiabatic coupling term τ as a function of φ encircling the CI. It can be readily seen that τ of the PIP-NN PEM is symmetric, while that the spline PEM is not quite correct near linearity. This is because the spline fit did not properly define V_{12} in the range of θ. The line integral of τ along φ over a circle around the CI is 3.141 592 for the PIP-NN PEM, as expected. The same geometric quantization is observed around the HHO CI as well, but the data are not shown here. It should be noted that the antisymmetric character of V_{12} has little impact on the outcomes of the photodissociation dynamics since the bending angle for three atom systems is always less than π in the calculation. As a result, the antisymmetry of V_{12} is usually ignored and has seldomly been discussed when constructing the diabatic PEM.

For the diabatic PEM of NH_3 system, it is much harder to fit the data in the full six dimensions since it needs to cover the large global configuration space. 19 835 points were chosen in the Franck-Condon region, near the CI, and in the dissociation asymptote from the Zhu-Yarkony (ZY) PEM.[68,82] To sample the points efficiently, some trial quantum dynamical calculations with different initial vibrational states were carried on the ZY PES, and the points with large population densities in the dissociation wavefunctions were chosen. An energy ceiling of 12 eV was set for accepting the chosen points for both two diagonal potentials V_{11} and V_{22}, and the value of cos θ was chosen to be larger than 0.0002 to avoid the linear singularity. We note in passing that no gradient was used in the fitting, which could in principle reduce the number of points needed for a faithful fit. All 22 PIPs up to the third order for the AB_3 system were used in the input layer of the NN and 40 neurons were used for both hidden layers, resulting in 2601 parameters. The final fitting RMSEs for the V_{11}, V_{22}, and V_{12} are 10.1, 10.2, and 3.2 meV, respectively. Figure 5 shows the fitting error distributions for V_{11}, V_{22}, and V_{12}, respectively.

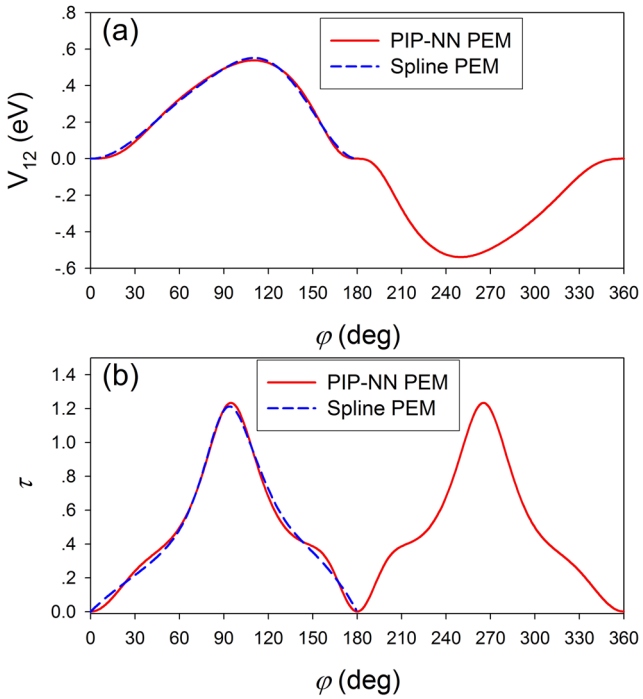

FIG. 4. The coupling term V_{12} (a) and the derivative coupling (b) along the loop encircling the HOH CI, obtained from the spline[67] and PIP-NN PEMs.

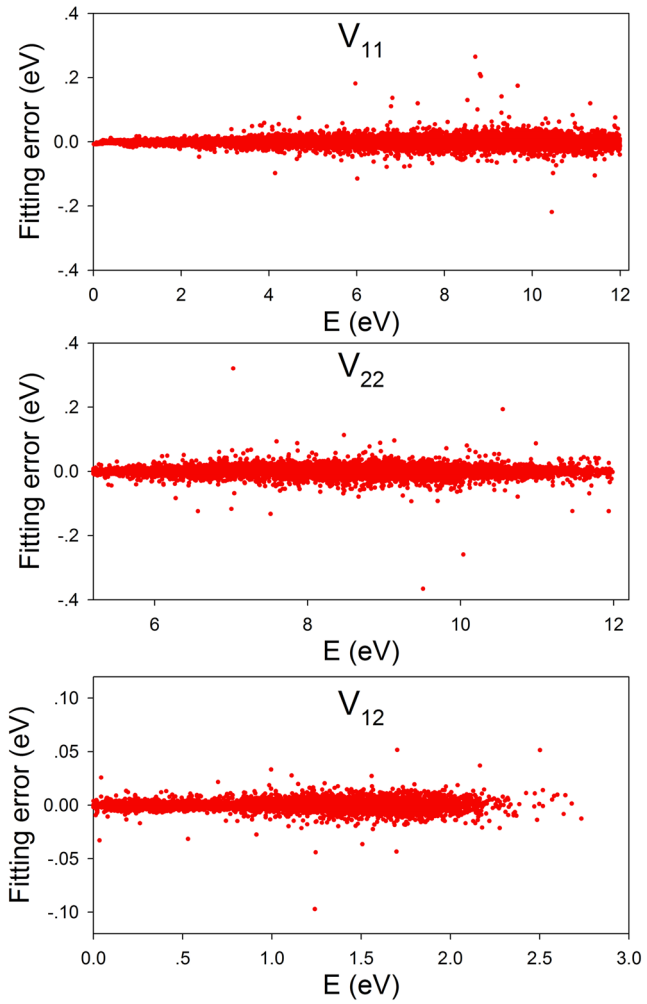

FIG. 5. Distributions of fitting errors for the V_{11}, V_{22}, and V_{12} of the NH_3 PEM.

The upper and middle panels of Fig. 6 show the adiabatic PESs in two coordinates obtained by diagonalizing the diabatic PEM. In the bottom panel, the coupling term V_{12} is compared for the PIP-NN and ZY PEMs. It can be seen that PIP-NN adiabatic PESs reproduce the topographies of the ZY ones very well, which validates the high accuracy of our PIP-NN fitting approach. Similarly, the difference in the coupling term is also very small.

To further test the fitting fidelity, we focus on the circular path for one H atom (H) to encircle the CI, which is denoted by an open circle in Fig. 1(b) and has the geometry of $R_{NH'} = R_{NH''} = 1.8$ bohr, $R_{NX} = 3.94$ bohr (X = H), and $\rho = 0.8$ bohr. The coupling term V_{12} and derivative coupling τ along the circle are compared for the ZY and PIP-NN PEMs in Figs. 7(a) and 7(b), respectively. It can be readily seen that they are in good agreement. In particular, the line integrals of τ along φ over the circle on both ZY and PIP-NN PEMs are essentially π within machine accuracy.

Furthermore, to validate the accuracy of the PIP-NN diabatic PEM, we calculated the absorption spectrum of the ground ro-vibrational initial state of $NH_3(\tilde{X})$ and the product $NH_2(\tilde{A})/NH_2(\tilde{X})$ branching ratio at the full-dimensional level. The six-dimensional Hamiltonian can be found in our earlier work.[83] It should be noted that the full-dimensional quantum dynamics calculations were done with the exponential basis set for the out-of-plane angle instead of the pure parity-adapted basis,[83] due to the antisymmetric character of the coupling term V_{12} (see Fig. 6). The parameters used in the dynamical calculations are listed in Table IV. It can be seen from the upper panel of Fig. 8 that the absorption spectra for both two initial parity states of $NH_3(\tilde{X})$, including the positions and widths of the peaks, on the PIP-NN PEM are all in excellent agreement with those on the ZY PEM, which suggests the high accuracy of the diabatic PIP-NN PEMs near the Franck-Condon region. The lower panel of Fig. 8 further compares the product $NH_2(\tilde{A})/NH_2(\tilde{X})$ branching ratio calculated on both PEMs. It can be also seen that the trend and main oscillatory structures of the branching ratio are well preproduced by the PIP-NN PEM, which suggests that the dissociation pathways and the intersection region between the two electronic states are well represented by the PIP-NN method as well.

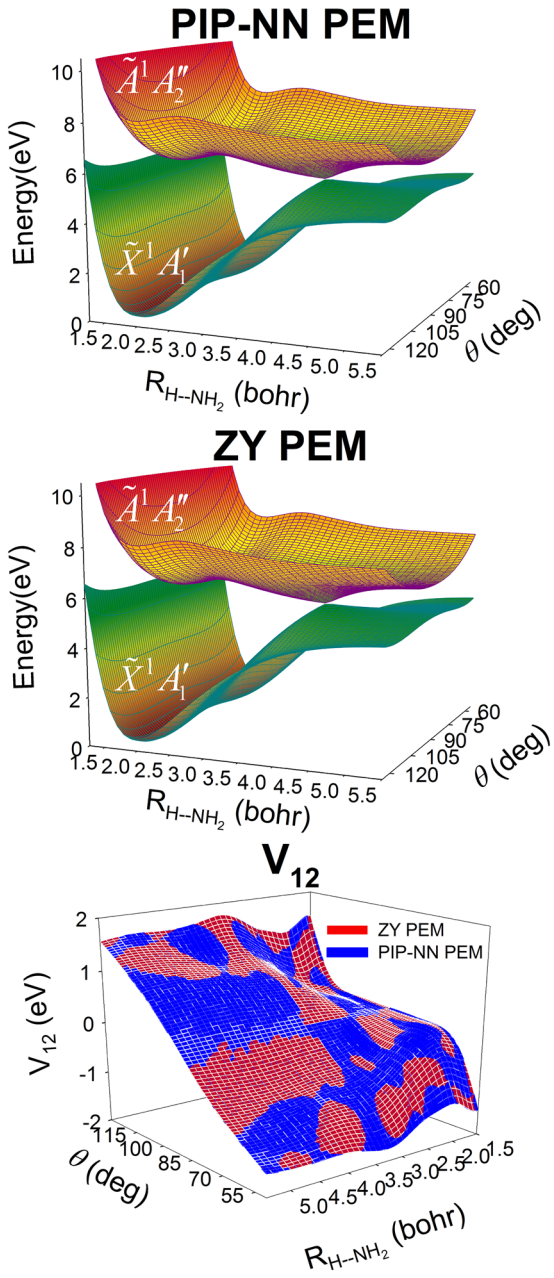

FIG. 6. Adiabatic PESs of NH_3 as a function of R(N–H) and out-of-plane angle θ (the angle between the C_{3v} axis and NH bond), obtained from the PIP-NN (upper panel) and ZY (middle panel) PEMs. The lower panel shows the comparison of the coupling term V_{12}.

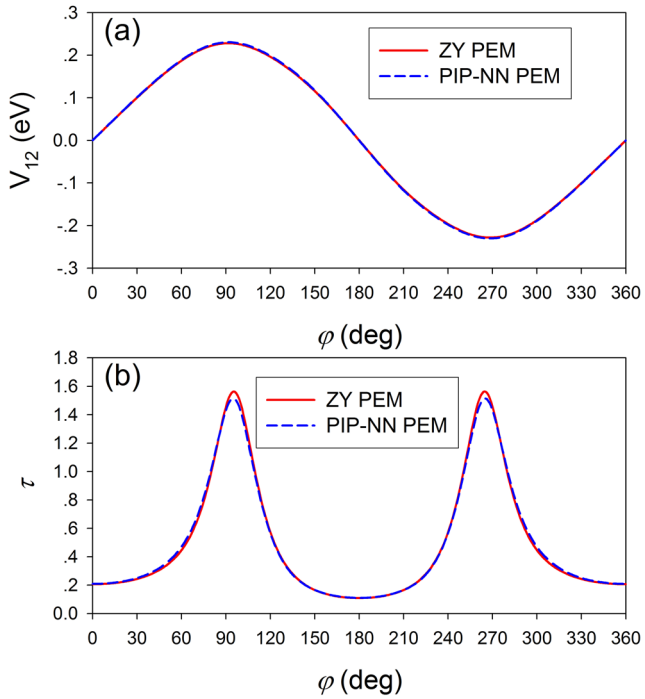

FIG. 7. Comparison of the coupling term V_{12} (a) and the derivative coupling (b) along the loop encircling the NH_3 CI obtained from the ZY and PIP-NN PEMs.

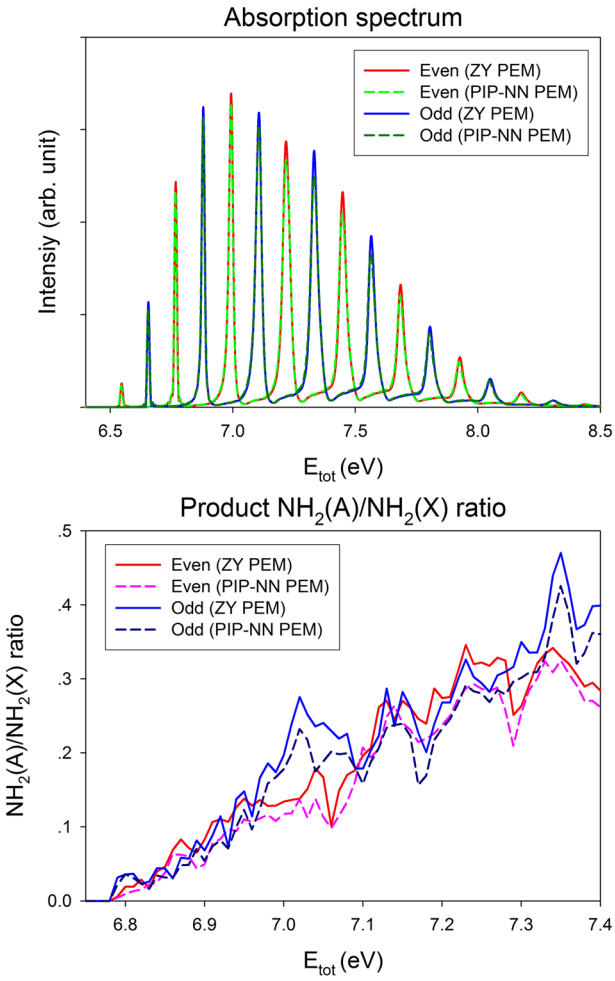

FIG. 8. Comparison of the calculated absorption spectrum (upper panel) and $NH_2(\tilde{A})/NH_2(\tilde{X})$ branching ratio (lower panel) as a function of the total energy (in eV) for the photodissociation of NH_3, obtained from the ZY and PIP-NN PEMs. "Even" and "Odd" symbols denote the even and odd parities of initial ro-vibrational states.

TABLE IV. Numerical parameters (in a.u.) used in wave packet calculations for the NH_3 photodissociation in the A band.

Grid/basis ranges and sizes
$r_3 \in [1.2, 14.0]$, $N_3 = 100$
$r_1 \in [1.2, 4.5]$, $r_2 \in [1.2, 4.5]$, for $1 \le i_3 \le 21$, $N_1 = N_2 = 21$;
for $22 \le i_3 \le 100$, $N_1 = N_2 = 5$
$N_{j_1} = N_{j_2} = 21$ over $[0°, 180°]$; $N_m = 41$ over $[-180°, 180°]$
Damping functions
$\exp[-0.006(r_3 - 10.6)^2]$, for $10.6 < r_3 < 14.0$
$\exp[-0.1(r_1 - 3.1)^2]$, for $3.1 < r_1 < 4.5$
$\exp[-0.1(r_2 - 3.1)^2]$, for $3.1 < r_2 < 4.5$
Chebyshev propagation steps: 12 000

IV. CONCLUSIONS

Non-adiabatic dynamics is a major current research frontier in chemical physics. An accurate characterization of the multi-state dynamics requires detailed knowledge of the coupled electronic and nuclear motion beyond the BO approximation. While non-adiabatic direct dynamics studies, which compute the forces as well as NACTs on the fly, shed valuable light on the non-adiabatic processes,[84,85] these studies are still based on electronic structure theory that is far from chemical accuracy. We have advocated a strategy in which the diabatic PEM is constructed with the highest level of electronic structure theory,[40,41] which not only is highly accurate but also facilitates quantum dynamics calculations.

In this work, we propose the use of a machine learning method, in particular, NNs, to represent the elements of a diabatic PEM. NNs have been successfully used to represent adiabatic PESs, but their applications to diabatic PEMs are rare. Our strategy here is to represent diabatic PEM elements with individual NNs, assuming that these have already been calculated using some forms of diabatization. Differing from adiabatic PESs, the off-diagonal elements of a PEM require special treatments concerning the permutation-inversion symmetry of the system, particularly around a CI seam. These symmetry considerations have been lacking in previous NN fits of diabatic PEMs. Such treatments are illustrated using two prototypical examples in which the photodissociation dynamics is strongly influenced by CIs. Our PIP-NN PEMs are shown to accurately capture the geometric phase of the corresponding CI. Our dynamical results on the new diabatic PEMs further confirm the accuracy of this PIP-NN approach. The efficiency can be further improved if gradients are included in the fitting. Finally, we note that the strategies concerning the symmetry adaptation can be extended straightforwardly to a more elaborate NN representation of diabatic PEMs, such as the direct fit of *ab initio* energies, gradients, and derivative couplings as done in the Zhu-Yarkony approach.[41] However, its application to larger systems requires more studies.

ACKNOWLEDGMENTS

H.G. and D.R.Y. acknowledge support from a grant from the Department of Energy (Grant No. DE-SC0015997).

[1] M. Born and K. Huang, *Dynamical Theory of Crystal Lattices* (Clarendon, Oxford, 1954).
[2] J. N. Murrell, S. Carter, S. C. Farantos, P. Huxley, and A. J. C. Varandas, *Molecular Potential Energy Functions* (Wiley, Chichester, 1984).
[3] T. Hollebeek, T.-S. Ho, and H. Rabitz, Annu. Rev. Phys. Chem. **50**, 537 (1999).
[4] M. A. Collins, Theor. Chem. Acc. **108**, 313 (2002).
[5] B. J. Braams and J. M. Bowman, Int. Rev. Phys. Chem. **28**, 577 (2009).
[6] J. Li, B. Jiang, H. Song, J. Ma, B. Zhao, R. Dawes, and H. Guo, J. Phys. Chem. A **119**, 4667 (2015).
[7] R. Dawes and S. A. Ndengué, Int. Rev. Phys. Chem. **35**, 441 (2016).
[8] M. Majumder, A. S. Ndengué, and R. Dawes, Mol. Phys. **114**, 1 (2016).
[9] C. Qu, Q. Yu, and J. M. Bowman, Annu. Rev. Phys. Chem. **69**, 151 (2018).
[10] L. M. Raff, R. Komanduri, M. Hagan, and S. T. S. Bukkapatnam, *Neural Networks in Chemical Reaction Dynamics* (Oxford University Press, Oxford, 2012).
[11] S. Manzhos, R. Dawes, and T. Carrington, Jr., Int. J. Quantum Chem. **115**, 1012 (2015).
[12] B. Jiang, J. Li, and H. Guo, Int. Rev. Phys. Chem. **35**, 479 (2016).
[13] J. Behler, J. Chem. Phys. **145**, 170901 (2016).
[14] B. Fu and D. H. Zhang, J. Chem. Theory Comput. **14**, 2289 (2018).
[15] J. Behler and M. Parrinello, Phys. Rev. Lett. **98**, 146401 (2007).
[16] J. Behler, J. Chem. Phys. **134**, 074106 (2011).
[17] B. Jiang and H. Guo, J. Chem. Phys. **139**, 054112 (2013).

[18]J. Li, B. Jiang, and H. Guo, J. Chem. Phys. **139**, 204103 (2013).
[19]K. Shao, J. Chen, Z. Zhao, and D. H. Zhang, J. Chem. Phys. **145**, 071101 (2016).
[20]B. Jiang and H. Guo, J. Chem. Phys. **141**, 034109 (2014).
[21]D. H. Zhang and H. Guo, Annu. Rev. Phys. Chem. **67**, 135 (2016).
[22]B. Fu, X. Shan, D. H. Zhang, and D. C. Clary, Chem. Soc. Rev. **46**, 7625 (2017).
[23]T. Yang, J. Chen, L. Huang, T. Wang, C. Xiao, Z. Sun, D. Dai, X. Yang, and D. H. Zhang, Science **347**, 60 (2015).
[24]M. L. Weichman, J. A. DeVine, M. C. Babin, J. Li, L. Guo, J. Ma, H. Guo, and D. M. Neumark, Nat. Chem. **9**, 950 (2017).
[25]J. A. DeVine, M. L. Weichman, B. Laws, J. Chang, M. C. Babin, G. Balerdi, C. Xie, C. L. Malbon, W. C. Lineberger, D. R. Yarkony, R. W. Field, S. T. Gibson, J. Ma, H. Guo, and D. M. Neumark, Science **358**, 336 (2017).
[26]D. Yuan, S. Yu, W. Chen, J. Sang, C. Luo, T. Wang, X. Xu, P. Casavecchia, X. Wang, Z. Sun, D. H. Zhang, and X. Yang, Nat. Chem. **10**, 653 (2018).
[27]D. R. Yarkony, Rev. Mod. Phys. **68**, 985 (1996).
[28]W. Domcke, D. R. Yarkony, and H. Köppel, *Conical Intersections: Electronic Structure, Dynamics and Spectroscopy* (World Scientific, Singapore, 2004).
[29]M. Baer, *Beyond Born-Oppenheimer: Electronic Nonadiabatic Coupling Terms and Conical Intersections* (Wiley, New Jersey, 2006).
[30]H. C. Longuet-Higgins, U. Öpik, M. H. L. Pryce, and R. A. Sack, Proc. R. Soc. A **244**, 1 (1958).
[31]C. A. Mead, Rev. Mod. Phys. **64**, 51 (1992).
[32]B. K. Kendrick, J. Phys. Chem. A **107**, 6739 (2003).
[33]I. G. Ryabinkin, L. Joubert-Doriol, and A. F. Izmaylov, Acc. Chem. Res. **50**, 1785 (2017).
[34]I. G. Ryabinkin and A. F. Izmaylov, Phys. Rev. Lett. **111**, 220406 (2013).
[35]C. Xie, J. Ma, X. Zhu, D. R. Yarkony, D. Xie, and H. Guo, J. Am. Chem. Soc. **138**, 7828 (2016).
[36]C. Xie, C. L. Malbon, D. R. Yarkony, D. Xie, and H. Guo, J. Am. Chem. Soc. **140**, 1986 (2018).
[37]H. Köppel, W. Domcke, and L. S. Cederbaum, Adv. Chem. Phys. **57**, 59 (1984).
[38]D. R. Yarkony, Chem. Rev. **112**, 481 (2011).
[39]J. E. Subotnik, E. C. Alguire, Q. Ou, B. R. Landry, and S. Fatehi, Acc. Chem. Res. **48**, 1340 (2015).
[40]H. Guo and D. R. Yarkony, Phys. Chem. Chem. Phys. **18**, 26335 (2016).
[41]X. Zhu and D. R. Yarkony, Mol. Phys. **114**, 1983 (2016).
[42]R. Abrol and A. Kuppermann, J. Chem. Phys. **116**, 1035 (2001).
[43]C. R. Evenhuis and M. A. Collins, J. Chem. Phys. **121**, 2515 (2004).
[44]X. Zhu and D. R. Yarkony, J. Chem. Phys. **132**, 104101 (2010).
[45]S. Mukherjee, S. Bandyopadhyay, A. K. Paul, and S. Adhikari, J. Phys. Chem. A **117**, 3475 (2013).
[46]H. J. Werner and W. Meyer, J. Chem. Phys. **74**, 5802 (1981).
[47]H. Nakamura and D. G. Truhlar, J. Chem. Phys. **115**, 10353 (2001).
[48]J. E. Subotnik, S. Yeganeh, R. J. Cave, and M. A. Ratner, J. Chem. Phys. **129**, 244101 (2008).
[49]C. E. Hoyer, X. Xu, D. Ma, L. Gagliardi, and D. G. Truhlar, J. Chem. Phys. **141**, 114104 (2014).
[50]A. Viel and W. Eisfeld, J. Chem. Phys. **120**, 4603 (2004).
[51]N. Wittenbrink, F. Venghaus, D. Williams, and W. Eisfeld, J. Chem. Phys. **145**, 184108 (2016).
[52]M. Baer, Chem. Phys. **15**, 49 (1976).
[53]C. A. Mead and D. G. Truhlar, J. Chem. Phys. **77**, 6090 (1982).
[54]C. R. Evenhuis, X. Lin, D. H. Zhang, D. Yarkony, and M. A. Collins, J. Chem. Phys. **123**, 134110 (2005).
[55]O. Godsi, C. R. Evenhuis, and M. A. Collins, J. Chem. Phys. **125**, 104105 (2006).
[56]Z. H. Li, R. Valero, and D. G. Truhlar, Theor. Chem. Acc. **118**, 9 (2007).
[57]V. C. Mota and A. J. C. Varandas, J. Phys. Chem. A **112**, 3768 (2008).
[58]X. Zhu and D. R. Yarkony, J. Chem. Phys. **136**, 174110 (2012).
[59]X. Zhu and D. R. Yarkony, J. Chem. Phys. **137**, 22A511 (2012).
[60]H. Ndome, R. Welsch, and W. Eisfeld, J. Chem. Phys. **136**, 034103 (2012).
[61]D. Opalka and W. Domcke, J. Chem. Phys. **138**, 224103 (2013).
[62]K. R. Yang, X. Xu, J. J. Zheng, and D. G. Truhlar, Chem. Sci. **5**, 4661 (2014).
[63]X. Zhu and D. R. Yarkony, J. Chem. Phys. **144**, 024105 (2016).
[64]T. Lenzen and U. Manthe, J. Chem. Phys. **147**, 084105 (2017).
[65]Y. Guan, B. Fu, and D. H. Zhang, J. Chem. Phys. **147**, 224307 (2017).
[66]B. Jiang, D. Xie, and H. Guo, J. Chem. Phys. **134**, 231103 (2011).
[67]B. Jiang, D. Xie, and H. Guo, J. Chem. Phys. **136**, 034302 (2012).
[68]X. Zhu, J. Ma, D. R. Yarkony, and H. Guo, J. Chem. Phys. **136**, 234301 (2012).
[69]J. Ma, X. Zhu, H. Guo, and D. R. Yarkony, J. Chem. Phys. **137**, 22A541 (2012).
[70]P. R. Bunker and P. Jensen, *Molecular Symmetry and Spectroscopy* (NRC Research Press, Ottawa, 1998).
[71]A. J. Dobbyn and P. J. Knowles, Mol. Phys. **91**, 1107 (1997).
[72]D. R. Yarkony, Mol. Phys. **93**, 971 (1998).
[73]Á. Vibók, G. J. Halász, S. Suhai, and M. Baer, J. Chem. Phys. **122**, 134109 (2005).
[74]M. I. McCarthy, P. Rosmus, H.-J. Werner, P. Botschwina, and V. Vaida, J. Chem. Phys. **86**, 6693 (1987).
[75]D. R. Yarkony, J. Phys. Chem. A **101**, 4263 (1997).
[76]G. J. Atchity, S. S. Xantheas, and K. Ruedenberg, J. Chem. Phys. **95**, 1862 (1991).
[77]C. L. Malbon, X. Zhu, H. Guo, and D. R. Yarkony, J. Chem. Phys. **145**, 234111 (2016).
[78]C. Xie, C. L. Malbon, D. R. Yarkony, and H. Guo, J. Chem. Phys. **147**, 044109 (2017).
[79]M. A. Collins and D. F. Parsons, J. Chem. Phys. **99**, 6756 (1993).
[80]Z. Xie and J. M. Bowman, J. Chem. Theory Comput. **6**, 26 (2010).
[81]M. T. Hagan and M. B. Menhaj, IEEE Trans. Neural Networks **5**, 989 (1994).
[82]C. Xie, J. Ma, X. Zhu, D. H. Zhang, D. R. Yarkony, D. Xie, and H. Guo, J. Phys. Chem. Lett. **5**, 1055 (2014).
[83]J. Ma, C. Xie, X. Zhu, D. R. Yarkony, D. Xie, and H. Guo, J. Phys. Chem. A **118**, 11926 (2014).
[84]L. Wang, A. Akimov, and O. V. Prezhdo, J. Phys. Chem. Lett. **7**, 2100 (2016).
[85]B. F. E. Curchod and T. J. Martínez, Chem. Rev. **118**, 3305 (2018).